doi.org/10.26434/chemrxiv.7468070.v1

Dynamic Order-Disorder Transition in the S = ½ Kagome Antiferromagnets Barlowite and Claringbullite

Alyssa Henderson, Lianyang Dong, Sananda Biswas, Hannah Revell, Yan Xin, John A. Schlueter, Roser Valenti, Theo Siegrist

Submitted date: 14/12/2018 • Posted date: 17/12/2018

Citation information: Henderson, Alyssa; Dong, Lianyang; Biswas, Sananda; Revell, Hannah; Xin, Yan; Schlueter, John A.; et al. (2018): Dynamic Order-Disorder Transition in the S = ½ Kagome Antiferromagnets Barlowite and Claringbullite. ChemRxiv. Preprint.

The nature of the structural phase transition in the quantum magnets barlowite, Cu4(OH)6FBr, and claringbullite, Cu4(OH)6FCl was investigated. These materials consist of parallel-stacked Cu2+ kagome layers, separated by planes that contain Cu2+ cations and halide anions. The structural transition is of an order-disorder type, where at ambient temperature the interlayer Cu2+ ions are disordered over three equivalent positions. In barlowite, the dynamic disorder becomes static as the temperature is decreased, resulting in a lowering of the overall symmetry from hexagonal P63/mmc to orthorhombic. The dynamic disorder in claringbullite persists to lower temperatures, with a transition to orthorhombic space group Pnma observed in some samples. Ab initio density functional theory calculations explain this temperature-dependent structural phase transition and provide additional insights regarding the differences between these two materials.

Dynamic Order-Disorder Transition in the *S* = ½ Kagome Antiferromagnets Barlowite and Claringbullite

Alyssa Henderson [1, 2], Lianyang Dong [2], Sananda Biswas[3], Hannah I. Revell [2], Yan Xin [2], John A. Schlueter[4], Roser Valenti[3], and Theo Siegrist [2,5]

[1]Department of Physics, Florida State University Tallahassee, FL 32310;
[2]National High Magnetic Field Laboratory 1800 E Paul Dirac Drive, Tallahassee, FL 32310
[3]Institute of Theoretical Physics, Goethe Universität Frankfurt am Main, Max von Laue Strasse 1, 60438 Frankfurt am Main, Germany
[4]Division of Material Research, National Science Foundation, 201 Wilson Boulevard, Arlington, Virginia 22230
[5]Department of Chemical and Biomedical Engineering, FAMU-FSU College of Engineering, Tallahassee, FL 32310

Supporting information for this article is given via a link at the end of the document.

Abstract: *The nature of the structural phase transition in the quantum magnets barlowite, $Cu_4(OH)_6FBr$, and claringbullite, $Cu_4(OH)_6FCl$ was investigated. These materials consist of parallel-stacked Cu^{2+} kagome layers, separated by planes that contain Cu^{2+} cations and halide anions. The structural transition is of an order-disorder type, where at ambient temperature the interlayer Cu^{2+} ions are disordered over three equivalent positions. In barlowite, the dynamic disorder becomes static as the temperature is decreased, resulting in a lowering of the overall symmetry from hexagonal $P6_3/mmc$ to orthorhombic. The dynamic disorder in claringbullite persists to lower temperatures, with a transition to orthorhombic space group Pnma observed in some samples. Ab initio density functional theory calculations explain this temperature-dependent structural phase transition and provide additional insights regarding the differences between these two materials.*

Quantum magnets, materials showing strong correlations and an *S* = ½ spin, exploit quantum mechanical functionality that is often counterintuitive and without equivalence in the classic world. In systems where competing interactions lead to frustration, quantum fluctuations remain strong even to the lowest temperatures. The ground state of such systems, in particular two-dimensional frustrated magnets, is considered the quantum spin liquid (QSL), where no long-range order exists even at *T* = 0 K.[1, 2] In addition, the proposed connection between high-temperature superconductivity and QSLs has been discussed extensively.[3-5] The expected long-range quantum entanglement and topological order in QSL materials therefore allow probing novel states of matter.[6, 7]

Condensed matter phases that realize a QSL provide a synthesis challenge in solid state chemistry.[8] The search has mostly focused on *S* = ½ two-dimensional spin systems in trigonal and kagome lattices, with antiferromagnetic interactions so that geometrical frustration is observed. Examples containing molecule-based *S* = ½ triangular spin lattices include κ-(BEDT-TTF)$_2$Cu$_2$(CN)$_3$ (BEDT-TTF = bis(ethylenedthio)tetrathia-fulvalene)[9] and EtMe$_3$Sb[Pd(dmit)$_2$]$_2$ (dmit = 1,3-dithiole-2-thione-4,5-dithiolate).[10] The molecular nature of these cation radical salts complicates their characterization and interpretation.[11] Alternatively, transition metal ions can also provide *S* = ½ systems. However, such systems are prone to distortions that relieve frustration, inducing long-range order at low temperatures. Herbertsmithite, $ZnCu_3(OH)_6Cl_2$, an *S* = ½ antiferromagnet, is one of the few geometrically perfect kagome lattices which shows strong evidence of a QSL state, where fractionalized spin excitations form a spectral continuum.[12, 13] Herbertsmithite belongs to the family of atacamite minerals with composition $Zn_xCu_{4-x}(OH)_6Cl_2$. For *x* = 0 (clinoatacamite), the metal sites between the distorted kagome layers are occupied by Cu^{2+} ions, mediating magnetic interactions between these layers, resulting in magnetic long range order. As interlayer Cu^{2+} ions are replaced by Zn^{2+} ions, geometrically perfect kagome layers are stabilized at *x* > 1/3 (Zn-paratacamite), whereas magnetic order is suppressed at *x* = 1.[14, 15] Single crystals of herbertsmithite have been grown successfully, a key step for further characterization of their magnetic behavior.[13, 16] Unfortunately, herbertsmithite has the potential for site-disorder, with Zn^{2+} ions substituting for Cu^{2+} in the kagome layer.[17]

Barlowite and claringbullite are two related atacamite minerals with similar kagome layers (Figure 1). Claringbullite, which was discovered in 1973,[18, 19] has the chemical formula $Cu_4(OH)_6FCl$. The bromide derivative, barlowite, $Cu_4(OH)_6FBr$, was discovered in 2010.[20] Similar to herbertsmithite, the kagome lattice in these minerals is formed by Cu^{2+} ions. In herbertsmithite, interlayer chloride anions coordinate to three Cu^{2+} ions and three hydroxyl hydrogen atoms. (Figure S1.) Replacement of half of these chloride ions with fluoride shifts the layer stacking so the electronegative fluoride ion resides in a hydrogen rich cavity. In barlowite and claringbullite, the kagome layers stack directly above each other without any lateral shift. (Figure S2) Strong H-F hydrogen bonding interactions provide the likely origin of the different layer alignments. Disordered Cu^{2+} cations and halide anions are located between the copper hydroxide-based kagome layers.

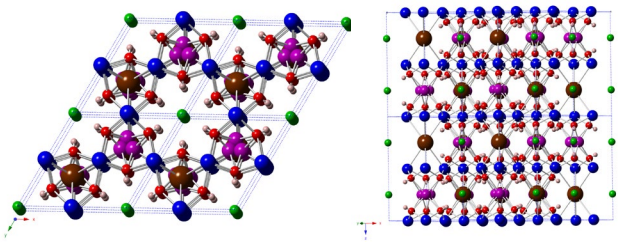

Figure 1. Packing diagram of barlowite, $Cu_4(OH)_6FBr$. Color scheme: Cu (Kagome layer) = blue, Cu (interlayer) = purple, O = red, H = salmon, Br = brown, F = green. (left) Illustration of the layer viewed along the *c*-axis. (right) Illustration of the layer packing. Claringbullite, $Cu_4(OH)_6FCl$, is isostructural, with the bromide ions replaced with chloride.

Synthetic barlowite, $Cu_4(OH)_6FBr$, has recently been prepared and characterized.[21-23] At room temperature, barlowite was reported to have a hexagonal structure,[21] while at low temperature, it was reported that the interlayer Cu^{2+} ions order,

inducing a small distortion of the kagome layers with a concomitant transition to a orthorhombic structure.[22] Because the room temperature hexagonal structure distorts to orthorhombic (ortho-hexagonal) at low temperature, we hypothesized that the low temperature static distortion due to interlayer Cu^{2+} cations becomes dynamic at an elevated temperature. In addition, the possibility of dynamic domain formation was considered. The synthesis of claringbullite, $Cu_4(OH)_6FCl$, was recently reported[24] and the room temperature hexagonal crystal structure reported to be isostructural to barlowite. These results led us to investigate the temperature dependence of the crystal structure of barlowite and claringbullite in order to understand their low-temperature induced structural distortions. Such lattice deformations are critical for the understanding the observed magnetic properties.

X-Ray Diffraction Studies

Barlowite. The reported room temperature crystal structure of barlowite[21] has disordered interlayer copper sites and a hexagonal unit cell, space group *P6₃/mmc*, with unit cell parameters *a* = 6.6786(2) Å and *c* = 9.2744(3) Å. These ambient temperature results were subsequently confirmed.[23] A recent single-crystal neutron diffraction study of barlowite indicated that the interlayer copper site is ordered at 100 K, resulting in an orthorhombic unit cell of symmetry *Cmcm*.[22] (Figures S3-S5) The unit cell parameters were found to be *a* = 6.665(13) Å, *b* = 11.521(2) Å ≈ √3*a*, and *c* = 9.256(18) Å. The same report indicated that the crystal structure determined at 110 K through single crystal X-ray diffraction has the same orthorhombic space group with *a* = 6.67 Å, *b* = 11.52 Å, and *c* = 9.26 Å. Based on powder neutron diffraction studies, a recent preprint claims the symmetry of barlowite to be *Pnma*, with unit cell parameters *a* = 11.551 Å, *b* = 9.280 Å, and *c* = 6.679 Å, for *T* = 250 K.[25] The reduction in symmetry from *Cmcm* to *Pnma* is due to a slightly different ordering scheme of the interlayer Cu atoms than described previously.[22]

In order to resolve the space group discrepancy among these results, room temperature powder X-ray diffraction data was collected at APS beamline 11-BM (ChemMatCARS). In agreement with the previously reported single crystal[21] and powder[23] X-ray diffraction data, this X-ray powder diffraction data did not show any signs of the orthorhombic distortion that is present at low temperature. The X-ray powder diffraction data was thus satisfactorily refined in GSAS-II[26] in hexagonal space group *P6₃/mmc* with disordered interlayer copper sites, resulting in an *R*-values of 0.082 (barlowite). (Figures S6). While the expected superstructure intensities are small compared to the hexagonal substructure intensities and thus difficult to observe even in synchrotron powder diffraction, the changes in the *a*- and *b*-axes are expected to result in observable peak broadening and splitting of the substructure reflections. However, in both barlowite and claringbullite, no such peak splitting/broadening is present at room temperature, rendering the structure metrically hexagonal.

As the above results suggested that a symmetry-breaking phase transition must occur between room temperature and 100 K in barlowite, a study was undertaken to investigate the appearance of superstructure reflections as a function of temperature. The superstructure reflection (-2, 0.5, 0) was determined to be a suitable marker for the identification of the hexagonal to orthorhombic distortion. This superstructure reflection is close to the substructure reflection (-2, 1, 0), a member of the (1, 1, 0) family of reflections, which served as an intensity reference. A (-2, *k*, 0) index scan from *k* = 0.4 to 1.1 therefore includes both reflections. Figure 2 shows the temperature dependence of intensity of the (-2, 0.5, 0) reflection compared to the (-2, 1, 0) reflection, indicating a "soft" onset of the Cu atom ordering at 276 K. The shape of the curve was checked on heating and cooling. It indicates further that short-range order is present up to about 285 K, where the superstructure intensity is of the order of the background. In addition, the substructure reflection (-2, 1, 0) shows the expected broadening due to the inequivalence of the *a*- and *b*-lattice parameters, growing more distinct as the temperature is lowered below 273 K.

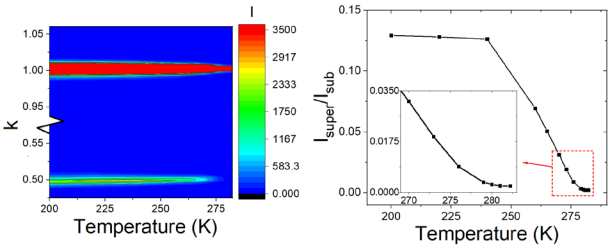

Figure 2. (Left) A (-2, *k*, 0) index scan from *k* = 0.4 to 1.1 for barlowite as a function of temperature. (Right) Temperature dependence of the integrated intensity of the superstructure reflection (-2, 0.5, 0) for a single crystal of barlowite, normalized to the (-2, 1, 0) intensity.

The orthorhombic distortion has several implications with respect to both crystal- and electronic-structure. The holosymmetric coordination of the interlayer Cu^{2+} ion[19] distorts to one of three positions at low temperature. This may be partially driven by more favourable coordination environments for the interlayer halide anions, including hydrogen bonding for fluorine. While the Jahn-Teller (JT) distortion has been extensively studied in octahedral Cu^{2+} complexes with 4+2 or 2+4 coordination, the JT effect can also occur in trigonal prismatic coordination.[27] We thus suggest that barlowite exhibits a dynamic JT distortion at room temperature.

The observed order-disorder transition in barlowite is likely influenced by the presence of defects that serve as nucleation centers for the orthorhombic phase and may lead to multiple twin formation. It is therefore expected that the transition temperature varies from sample to sample, and will be different for crystals grown by different methods. Furthermore, high cooling rates may lead to supercooling effects.

Claringbullite. Single crystals of claringbullite, $Cu_4(OH)_6FCl$, were investigated by single crystal X-ray diffraction at room temperature (295 K) and 110 K, using an Oxford Diffraction CCD system. The observed unit cell at 295 K is hexagonal, *P6₃/mmc*, with *a* = 6.6699(2) Á and *c* = 9.1761(3) Á. No superstructure reflections were observed between room temperature and 120 K. Analogous to barlowite, the structure is characterized by a Cu based kagome lattice (Wyckoff position 12c) and disordered interlayer Cu^{2+} ions. The interlayer Cu ions are found to be displaced from the ideal Wyckoff position 4b, and occupy the same off-center locations in their coordination octahedron. The kagome lattice is also stacked without any relative displacement, a result of the hydrogen bonding between the hydroxyl hydrogen atoms and fluorine atoms.

Similar to the case of barlowite (described above) powder the X-ray diffraction pattern measured on the APS beamline 11-BM at room temperature was further analyzed for a structural model in space group $P6_3/mmc$ and an ortho-hexagonal cell with

symmetry *Cmcm* and lattice parameters a = 6.6699 Å, $b = \sqrt{3}a$ = 11.5526 Å, and c = 9.1761 Å. Rietveld refinements using GSAS-II[26] clearly show that the structural model in *Cmcm* leads to superstructure intensities and resolved splitting of (*hk*0) reflections,[22] features not observed for claringbullite at room temperature (Figure S7), ruling out the orthorhombic structure model.

In contrast to barlowite, claringbullite does not show superstructure reflections at 120 K using our laboratory diffractometer. We therefore measured three single crystals of claringbullite at 100 K and 10 K at the APS ChemMatCARS beamline. In one case, no superstructure reflections were observed at a temperature of 10 K, with the symmetry remaining hexagonal $P6_3/mmc$. Two samples of claringbullite showed superstructure intensities at 100 K respectively consistent with a single- and a multiple-domain ortho-hexagonal unit cell. Careful examination of the diffraction frames showed that in the case of the single domain crystal, weak superstructure reflections violating *C*-centering of the orthorhombic unit cell are clearly present, leading to space group *Pnma* and unit cell parameters of a = 11.5133(2) Å, b= 9.1527(2) Å, and c = 6.6726(1) Å. In this setting, the hexagonal *c*-axis is now the *b*-axis, and the pseudo-hexagonal *a*-axis is $a/\sqrt{3}$ = 6.647 Å. The interlayer Cu atoms are now ordered, occupying one of the three sites above/below the triangle formed by the copper atoms in the kagome layers. In addition, there is a small puckering of the kagome layer, of the order of 0.12 Å. The correlated displacement of the interlayer Cu atoms is indicated by arrows in Figure 3. Results of the refinement are given in Table S2-S4 in the supplementary material.

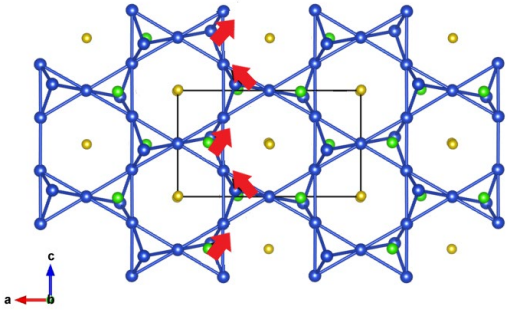

Figure 3. Claringbullite crystal structure at 100 K in space group *Pnma*. Cu-Cu bonds are indicated. Color scheme: Blue = Cu,, Yellow = F, Green = Cl. Hydrogen and Oxygen atoms have been omitted for clarity.

Scanning Transmission Electron Microscopy

The crystal structure of claringbullite was further investigated through the use of scanning transmission electron microscopy (STEM) studies. High angle annular dark field (HAADF) STEM imaging along and perpendicular to the hexagonal *c*-axis was carried out at room temperature. Through analysis of HAADF-STEM images, atomic structures can be directly and intuitively revealed. Atoms appear as bright dots with their intensity proportional to the square of atomic number (Z^2) and sample thickness. Figure 4a and 4b show the structure in projection parallel to the *c*-axis, revealing the kagome lattice in claringbullite. The brighter atomic columns are the Cu atoms in the kagome lattice layer. The weak intensity atoms (indicated by arrows in Figure 4b), which have triangle shapes cornered by three kagome Cu are the interlayer Cu. This indicates that the interlayer Cu^{2+} ions are in effect randomly distributed over the three possible sites. Looking at the structure perpendicular to *c*-axis, *i.e.* along the *a*-axis, as shown in Figure 4c-4e further proves this. The kagome Cu atoms in line 1 show high and low intensity as expected in the projection along the *a*-axis, ([10-10] projection, Figure 4), where some kagome Cu atoms have a distance of 8.8 Å along the electron beam direction, therefore showing brighter intensity. Adjacent Cu columns have an atomic distance of 17.6 Å, so they show lower intensity. Kagome Cu atoms along the beam direction have a width of 0.92 Å (Figure 4d), which is consistent with the width of a single atomic column with the microscope resolution of 0.78 Å. However, the width of the interlayer Cu site of 1.83 Å (Fig. 4e) is significantly broader, and is due to the random distribution of the interlayer Cu ions over the three possible positions. The projection of these interlayer Cu locations shows that they are separated by only 0.4 Å. Thus, the interlayer Cu ions exhibit a much wider intensity profile than those in the kagome layer.

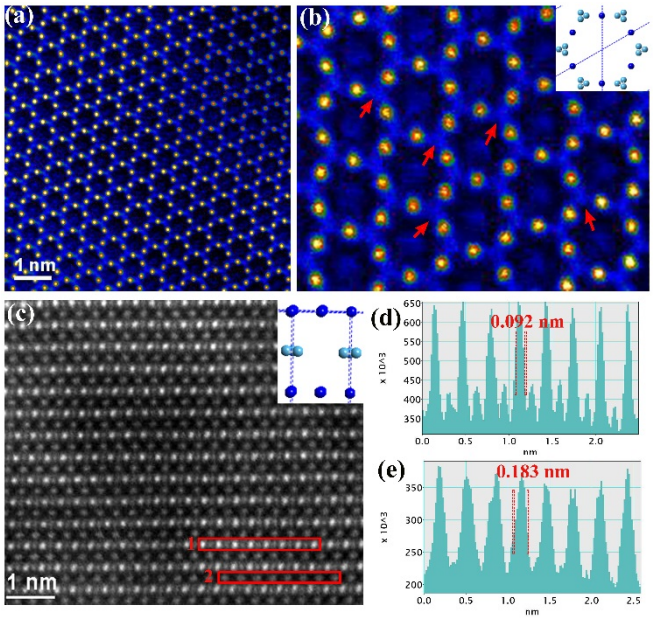

Figure 4. (a) Atomic resolution HAADF-STEM image looking down [0001] *c*-axis; (b) Enlarged and FFT -filtered [0001] image with selected interlayer Cu indicated by arrows; inset: corresponding projected structure schematic with kagome Cu as dark blue and interlayer Cu as light blue; (c) FFT-filtered atomic resolution images of [10-10] *a*-axis HAADF-STEM image; inset: corresponding schematic of projected structure; (d) Intensity line profile of line 1 of kagome Cu layer; (e) Intensity line profile of line 2 of interlayer Cu.

Ab-initio Calculations

In order to obtain the potential energy surface (PES) for the interlayer Cu atoms, static density functional theory (DFT) calculations were performed in the nonmagnetic configuration considering both the room temperature (symmetry $P6_3/mmc$) and the low temperature structure (symmetry *Cmcm*) parameters. The fractional occupancy of the interlayer Cu for the room temperature structure was removed in order to obtain the symmetry of the PES. For both systems a PES was obtained for each structure by comparing the total energy, due the nuclear motion of the interlayer Cu atoms on the plane containing halogen atoms, relative to a high symmetry position P (Figure 5). All other atoms were kept fixed at the experimentally obtained positions. These fixed positions were taken from data reported in this paper, except for barlowite at low temperature, for which literature coordinates[22] were utilized. By obtaining energies

along different paths away from P, it was found that the lowest energy structures always lie along either PA, PB or PC (Figure 5); where A, B and C denote the projected positions of three nearest Cu atoms (situated on the Kagome layer) from the position P, on the plane containing P and halogen atoms. We henceforth report the energies only along these three directions. However, schematics of full PESs which mimic the real calculations are shown in Figure 5a-b. Note that due to the broad temperature range used for the current study, magnetic moments might be quenched at high temperature (our magnetic calculations supports this view). Another factor which might affect the magnetic moment is the structural relaxation; our calculation of structural relaxation distorts the whole structure at low temperature as was suggested previously.[28] However, in order to enable comparison of the different PESs, the PESs were restricted to those obtained from nonmagnetic calculations.

The room temperature PES (Figure 5) reveals the three-fold symmetry which compels both claringbullite and barlowite to undergo an order-disorder transition as observed in the experiment due to the finite probability of tunnelling of the interlayer Cu atoms between three equivalent minima. Figure 5a clearly shows the degeneracy along PA, PB and PC. Though the other directions remain energetically higher, they still mimic the symmetry of the PES. The tunnelling frequency for an interlayer Cu was extracted by fitting a potential of the form $V(x) = -Ax^2+Bx^4$ to the curve in Figure 5c and solving an effective one-dimensional anharmonic oscillator problem. The values of tunnelling frequency thus obtained were 9.6 meV/f.u. and 13 meV/f.u. for barlowite and claringbullite, respectively.

Our experimental results suggest the order-disorder transition occurs at a lower temperature in claringbullite than in barlowite. Our result for the PES of the low temperature structure (symmetry *Cmcm*) supports this view (Figure 5d). We observe two distinctly different features from the room temperature PES: (1) low temperature PES is asymmetric as the degeneracy gets lifted along PA and PB/PC (the degeneracy along PB and PC remains), and (2) the energy barrier between the two lowest minima (shown by the black arrows), ΔE^* is one order of magnitude higher in the case of barlowite [~12 meV/(f.u.)] than in claringbullite (~2.3 meV/f.u.). This clearly shows that due to the breaking of the three-fold symmetry of PES, the system undergoes ordering. One might also observe here that the minimum for barlowite is along PA, while for claringbullite it is along PB/PC; however, as the value of ΔE^* for claringbullite is of the order of the error bar of our calculations, it is impossible to resolve the directional dependency of the energy minimum for claringbullite at low temperature. Our low temperature orthorhombic structure shows that the position PA is also favored in claringbullite, analogous to barlowite. As mentioned in the Supplementary information, we have considered the *Cmcm* symmetry for the low temperature structures; however, we have additionally performed one calculation to verify the energetics of the low-temperature structure of barlowite with *Cmcm* and *Pnma* (structure from Ref. 25) to find that the *Pnma* is lower in energy by 38 meV per Cu atom than *Cmcm*. As all our calculations are performed at $T = 0$ K, this implies that at a very low temperature, *Pnma* will win over *Cmcm*. Therefore, based on this result, we cannot rule out the possibility of *P63/mmc-Cmcm-Pnma* transition in these materials.

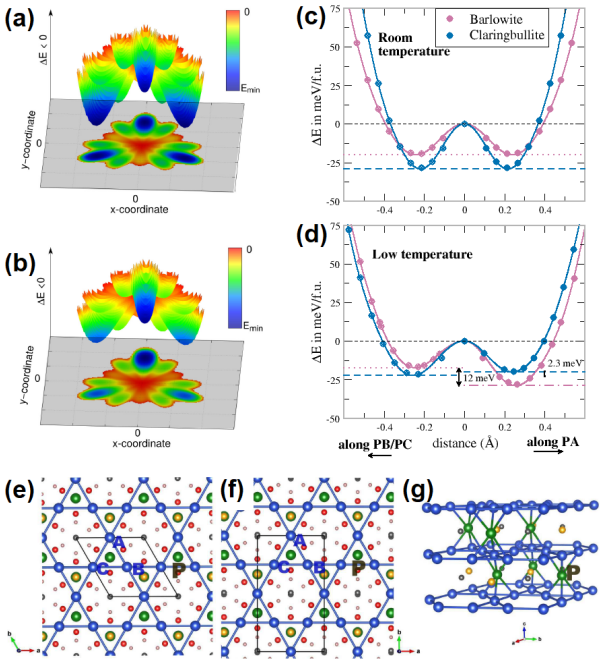

Figure 5. The potential energy surface (PES) at high (a) and low (b) temperatures show the schematic of the three-dimensional PES, whereas (c) and (d) show a cut through the PES at the high temperature and low temperature, respectively. A, B, C denote the symmetry paths along which the interlayer Cu atom at has been displaced in the plane containing the halogen atom. P is the high symmetric position of interlayer Cu (see text for further description). Top views of the Kagome planes in barlowite in *P6₃/mmc* (e) and *Cmcm* (f) geometry. The blue and green atoms are the Cu atoms belonging to the Kagome (blue atoms) and interlayer plane (green atoms), respectively. (g) shows the side view of Cu network. The unit-cell used for calculation is shown by the black lines. Note here that the interlayer Cu atoms were placed at the (hypothetical) highly symmetric position P in order to explain the potential energy surface (PES) later. A, B and C denote the projection of the three nearest Cu ions on the Kagome layer on the plane containing P. Grey, yellow, red and pink spheres indicate F, Cl/Br, O and H atoms.

Finally, we investigated the electronic structure in order to find the origin of the order-disorder transition in these systems; for this study we choose barlowite. The results suggest that these materials undergo a 'Jahn-Teller like distortion' due to the instability caused by the electronic degeneracy between two sets of *d*-orbitals of the interlayer Cu^{2+} ion at the position P with point group symmetry C_{3v} (Figure S8). Thus, the system becomes unstable with respect to the nuclear motion away from P in such a way that this degeneracy is lifted.

Since the order-disorder transition may be considered as a transition from a dynamic to a static Jahn-Teller distortion, the details of the coordination of the interlayer Cu atom is as follows: The Cu-O coordination polyhedron is trigonal prismatic, with the Cu offset towards one side, resulting in four short bonds with distances of 1.988 Å, and two longer Cu-O bonds at 2.434 Å. Distances to the three Cu atoms each in the kagome layers above and below are two distances of 2.737 Å, and four distances of 3.161 Å. This type of distortion was described previously for the case of trigonal prismatic Cu^{2+}, and it has the elongated bonds in the *cis* positions.[29] In the case of barlowite, similar Cu-O distances are observed, with similar distortions. However, the static distortion is favored in barlowite, whereas in claringbullite, the dynamic distortion prevails to lower temperatures, clearly favored due to the much higher barrier for ordering.

Conclusions

We have demonstrated that the room temperature structures of the kagome systems barlowite and claringbullite show dynamic disorder of the interlayer Cu^{2+} ions, rendering the kagome lattice of spin ½ Cu^{2+} ions perfectly hexagonal. A transition from dynamic disorder to static order occurs at 276 K for barlowite, where the symmetry is lowered from hexagonal *P6₃/mmc* to orthorhombic (*Cmcm* or *Pnma*) and the unit cell acquires a small distortion in the hexagonal (*ab*)-plane, slightly distorting the kagome lattice of Cu^{2+} atoms. This is in contrast to claringbullite, where this expected transition to the lower symmetry *Pnma* in an ortho-hexagonal unit cell is at a temperature below 110 K, or even below 10 K, below the magnetic transition temperature for selected samples. The calculated energy barriers for the transition from dynamic disorder to static order are 20.1 meV/f.u. for barlowite, and 35.1 meV/f.u. for claringbullite respectively, and the PES asymmetries are larger in barlowite than claringbullite, indicating that claringbullite will remain disordered to lower temperatures than barlowite. Defects present in a crystal may serve as nucleation centers for the order-disorder transition, resulting in different transition temperatures that depend on sample preparation, and potentially on cooling rates, and the history of the sample. While the two systems, barlowite and claringbullite, are almost identical, the substitution of Br for Cl clearly affects the behavior of the interlayer Cu^{2+} ion in a profound way.

Acknowledgements

We thank Dr. Lianyang Dong for assistance with data collection at ChemMatCARS and Dr. S. Winter for helpful discussions. NSF's ChemMatCARS Sector 15 is principally supported by the Divisions of Chemistry (CHE) and Materials Research (DMR), National Science Foundation, under grant number NSF/CHE-1346572. Use of the Advanced Photon Source, an Office of Science User Facility operated for the U.S. Department of Energy (DOE) Office of Science by Argonne National Laboratory, was supported by the U.S. DOE under Contract No. DE-AC02-06CH11357. J.A.S. acknowledges support from the Independent Research/Development program while serving at the National Science Foundation. Some of the work was carried out at the National High Magnetic Field Laboratory which is supported by the National Science Foundation under grant DMR-1644779 and the State of Florida. A.H., L.D. and T.S. acknowledge funding from the National Science Foundation under grant DMR-1534818 and DMR-1849539. H.I.R. thanks the NHMFL for the summer internship.

Keywords: barlowite • claringbullite • crystal structure • scanning transmission electron microscopy • ab initio calculation

[1] P. W. Anderson, *Mat. Res. Bull.* **1973**, *8*, 153.
[2] L. Balents, *Nature* **2010**, *464*, 199.
[3] P. A. Lee, *Science* **2008**, *321*, 1306.
[4] P. A. Lee, *Rep. Prog. Phys.* **2008**, *71*, 012501.
[5] B. J. Powell, R. H. McKenzie, *Rep. Prog. Phys.* **2011**, *74*, 056501.
[6] P. W. Anderson, *Science* **1987**, *235*, 1196.
[7] L. B. Ioffe, M. V. Feigel'man, A. Isoselevich, D. Ivanov, M. Troyer, G. Blatter, *Nature* **2002**, *415*, 503.
[8] A. P. Ramirez, *Nature Phys.* **2008**, *4*, 442.
[9] Y. Shimizu, K. Miyagawa, K. Kanoda, M. Maesato, G. Saito, *Phys. Rev. Lett.* **2003**, *91*, 107001.
[10] T. Itou, A. Oyamada, S. Maegawa, M. Tamura, R. Kato, *Phys. Rev. B* **2008**, *77*, 104413.
[11] K. Kanoda, R. Kato, *Annu. Rev. Condens. Matter Phys.* **2011**, *2*, 167.
[12] M. P. Shores, E. A. Nytko, B. M. Bartlett, D. G. Nocera, *J. Am. Chem. Soc.* **2005**, *127*, 13462.
[13] T. H. Han, J. S. Helton, S. Chu, A. Prodi, D. K. Shingh, C. Mazzoli, P. Muller, D. G. Nocera, Y. S. Lee, *Phys. Rev. B* **2011**, *83*, 100402.
[14] P. Mendels, F. Bert, *J. Phys. Soc. Jpn.* **2010**, *79*, 011001.
[15] M. A. de Vries, K. V. Kamenev, W. A. Kockelmann, J. Sanchez-Benitez, A. Harrison, *Phys. Rev. Lett.* **2008**, *100*, 157205.
[16] T.-H. Han, J. S. Helton, S. Chu, D. G. Nocera, J. A. Rodriguez, C. Broholm, Y. S. Lee, *Nature* **2012**, *492*, 406.
[17] D. E. Freedman, T. H. Han, A. Prodi, P. Muller, Q.-z. Huang, Y.-s. Chen, S. M. Webb, Y. S. Lee, T. M. McQueen, D. G. Nocera, *J. Am. Chem. Soc.* **2010**, *132*, 16185.
[18] E. E. Fejer, A. M. Clark, A. G. Couper, C. J. Elliott, *Mineralogical Magazine* **1977**, *41*, 433.
[19] P. C. Burns, M. A. Cooper, F. C. Hawthorne, *Can. Mineral.* **1995**, *33*, 633.
[20] P. A. Williams, F. Hatert, M. Pasero, S. J. Mills, *Mineralogical Magazine* **2010**, *74*, 797.
[21] T.-H. Han, J. Singleton, J. A. Schlueter, *Phys. Rev. Lett.* **2014**, *113*, 227203.
[22] C. M. Pasco, B. A. Trump, T. T. Tran, Z. A. Kelly, C. Hoffmann, I. Heinmaa, R. Stern, T. M. McQueen, *Physical Review Materials* **2018**, *2*, 044406.
[23] R. W. Smaha, W. He, J. P. Sheckelton, J. Wen, Y. S. Lee, *J. Solid State Chem.* **2018**, *268*, 123.
[24] X. Y. Yue, Z. W. Ouyang, J. F. Wang, Z. X. Wang, Z. C. Xia, Z. Z. He, *Phys. Rev. B* **2018**, *97*, 054417.
[25] K. Tustain, G. J. Nilsen, C. Ritter, I. da Silva, L. Clark, **2018**, arXiv:1810.01684v1.
[26] B. H. Toby, R. B. Von Dreele, *J. Appl. Cryst.* **2013**, *46*, 544.
[27] J. Echeverría, E. Cremades, A. J. Amoroso, S. Alvarez, *Chem. Commun.* **2009**, 4242.
[28] K. M. Ranjith, C. Klein, A. A. Tsirlin, H. Rosner, C. Krellner, M. Baenitz, *Sci. Rep.* **2018**, *8*, 10851.
[29] J. Echeverria, E. Cremades, A. J. Amoroso, S. Alvarez, *Chem. Commun.* **2009**, *0*, 4242

The nature of the structural phase transition in the quantum magnets barlowite, $Cu_4(OH)_6FBr$, and claringbullite, $Cu_4(OH)_6FCl$ was investigated through the use of X-ray diffraction, scanning transition electron microscopy, and *ab initio* calculations.

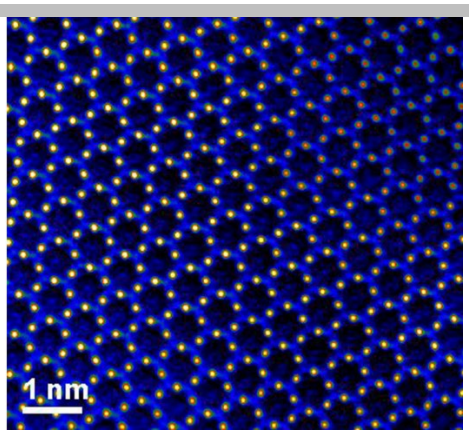

Alyssa Henderson, Lianyang Dong, Sananda Biswas, Hannah I. Revell, Yan Xin, John A. Schlueter, Roser Valenti, and Theo Siegrist**

Page No. – Page No.

Title

Supporting Information

Dynamic Order-Disorder Transition in the *S* = ½ Kagome Antiferromagnets Barlowite and Claringbullite

Alyssa Henderson, Lianyang Dong, Sananda Biswas, Hannah I. Revell, Yan Xin, John A. Schlueter, Roser Valenti, and Theo Siegrist**

Table of Contents

Experimental Procedures

Synthesis

Hydrothermal reactions were performed by combining CuO (6 mmol, 477 mg), CuF_2 (1 mmol, 102 mg), and $CuCl_2{\cdot}2H_2O$ (1 mmol, 170 mg or 0.5 mmol 86 mg) or $CuBr_2$ (1 mmol, 220 mg or 0.5 mmol, 110 mg) in 23 mL Parr General Purpose Acid Digestion Vessels, for claringbullite and barlowite respectively. It was found that less $CuCl_2{\cdot}2H_2O$ would often yield larger single crystals. The contents of the autoclave were heated for 100 hours at 150 °C, cooled to room temperature over 24 hours. The result in both cases was an aqua blue mixture at the bottom of the vessel, which was poured onto filter paper, dried, and collected. Both barlowite and claringbullite powder and single crystals were synthesized within each respective reaction.

Larger single crystals of claringbullite were prepared through use of seed crystals, as described earlier.[1] In a typical reaction, a mixture of $CuO:CuF_2:CuCl_2$ in a 6:1:1 molar ratio was placed in a 23 ml Parr vessel with 15 mL of water. Seed crystals were added to the vessel, which was then heated at 170 °C for 72 hours. Repeating this process over seven cycles resulted in the growth of crystals larger than 0.5 mm.

In order to prepare polycrystalline powders of claringbullite, a solution method was developed. In a Teflon cup, NH_4F (8 mmol, 133.8 mg) and NaOH (6 mmol, 108.4 mg) were dissolved in 20 mL water. In a second cup, $CuCl_2{\cdot}2H_2O$ (4 mmol, 308 mg) was dissolved in 10 mL water. Upon combination, 163.7 mg (29.6% yield) of claringbullite polycrystalline powder formed. The claringbullite powder was subsequently separated from the water via filtration, and dried in an oven at 30 °C.

[1] C. M. Pasco, B. A. Trump, T. T. Tran, Z. A. Kelly, C. Hoffmann, I. Heinmaa, R. Stern, T. M. McQueen, *Physical Review Materials* **2018**, *2*, 044406.

Table S1. Details of starting stoichiometry of single crystals studied using the APS ChemMatCARS beamline.

Sample	CuO	CuF_2	$CuCl_2{\cdot}2H_2O$	Temp, time	mL
C_01	6mmol, 473 mg	1mmol, 101 mg	½ mmol, 85 mg	150C, 100h	20
C_02	6mmol, 477 mg	1mmol, 100 mg	1mmol, 170 mg	150C, 100h	19
C_28	6mmol, 476 mg	1mmol, 101 mg	½ mmol, 86 mg	150C, 100h	20
B_05	6mmol, 480 mg	1mmol, 101 mg	CuBr: ½ mmol, 114mg	150C, 100h	20

Structural Characterization

Powder X-ray diffraction. Structural studies were carried out on polycrystalline materials through use of a Scintag PAD-V powder diffractometer with diffracted beam monochromator, Further room temperature structural studies used the mail-in program at the Advanced Photon Source (APS) beam line 11-BM for powder diffraction.

Single-crystal x-ray diffraction. The structure of single crystals were analyzed using an Oxford Diffraction Xcalibur-2 CCD diffractometer with graphite monochromated MoKα radiation and a Croyjet temperature control system operating in the range of 110 to 300 K to collect integrated intensities for structural refinements., A custom 4-circle Huber diffractometer in triple axis mode using graphite monochromators was used to follow specific reflection profiles and intensities in the temperature range of 200 to 300 K.

Structural characterization of microcrystals of barlowite and claringbullite were performed at both 10 K and 100 K at the ChemMatCARS sector 15 beamline of the Advanced Photon Source (APS) using a wavelength of 0.41328 Å, through use of a Bruker D8 diffractometer equipped with a PILATUS3 X CdTe 1M detector. Details of starting stoichiometry of single crystals studied are shown in Table S1. The structure of claringbullite sample C_01 was solved at 100 K and refinement details are shown in Tables S2-S4. Additional twinning was present in the same sample at a temperature of 10 K.

CCDC 1882561 (claringbullite, *Pnma*, temperature 100K, single crystal), 1883264 (claringbullite, *$P6_3/mmc$,* temperature 295K, powder), 1883276 (barlowite, *$P6_3/mmc$,* temperature 295K, powder), and 1019246 (barlowite, temperature 295K, single crystal) contain the supplementary crystallographic data for this paper. These data are provided free of charge by The Cambridge Crystallographic Data Centre.

Electron microscopy studies. Claringbullite was also analyzed through use of atomic resolution high angle annular dark field scanning transmission electron microscopy (HAADF-STEM) with a probe-aberration-corrected cold field-emission JEOL JEM-ARM200cF microscope operating at 200 kV at room temperature. The STEM resolution of the microscope is 0.78 Å. The images were taken with a probe size of 0.078 nm, a condenser lens aperture of 30 μm, scan speed of 32 μs/pixel, and camera length 8 cm, which corresponds to a probe convergence angle of 21 mrad and collection angle of 68 mrad.

Table S2: Structural refinement information for x-ray diffraction data collected on claringbullite crystal C_01 at the ChemMatCARS beamline.

Structure	
Formula	$Cu_4(OH)_6FCl$
Symmetry	*Pnma* #62
a	11.5133(2) Å
b	9.1527(2)Å
c	6.6727(2) Å
Z	4
Volume	703.144(2) $Å^3$
Reflections total	28695
Reflections unique	2016
θ_{min}	2.05°
θ_{max}	22.19°
$\lambda(synchrotron)$	0.41328
R_{all}	0.092
wR_{obs}	0.067

Table S3: Atomic positions and U_{eq} [$Å^2$]

atom	type	x	y	z	Ueq
Cu1	Cu	0.5000	0.5000	0.0000	0.0043
Cu2	Cu	0.24927(2)	0.48655(3)	−0.24478(4)	0.0043
Cu3	Cu	0.31469(4)	0.7500	−0.05991(7)	0.0063
O4	O	0.39723(14)	0.90894(17)	−0.1981(2)	0.0041
O5	O	0.40210(14)	0.91216(18)	0.1970(2)	0.0047
O6	O	0.20142(15)	0.59463(18)	−0.0023(2)	0.0049
Cl7	Cl	0.32787(8)	0.2500	−0.00979(11)	0.0083
F8	F	0.5029(2)	0.7500	−0.4929(3)	0.0087

Table S4: Anisotropic thermal parameters [$Å^2$]

atom	u11	u22	u33	u12	u13	u23
Cu1	0.00131(17)	0.00476(18)	0.00687(18)	0.00042(11)	0.00011(11)	0.00203(13)
Cu2	0.00133(12)	0.00454(12)	0.00697(14)	−0.00193(9)	0.00029(9)	−0.00090(9)
Cu3	0.00383(17)	0.00221(16)	0.01292(19)	0.0000	0.00127(14)	0.0000
O4	0.0016(6)	0.0027(6)	0.0078(7)	−0.0001(5)	0.0009(5)	−0.0017(5)
O5	0.0013(6)	0.0046(7)	0.0082(7)	0.0031(5)	0.0015(5)	−0.0003(5)
O6	0.0018(7)	0.0033(7)	0.0097(7)	0.0005(5)	0.0008(5)	0.0009(5)
Cl7	0.0070(3)	0.0051(3)	0.0127(3)	0.0000	−0.0004(2)	0.0000
F8	0.0039(9)	0.0114(10)	0.0106(9)	0.0000	0.0016(6)	0.0000

Ab inito calculations

Total-energy calculations are performed using density functional theory (DFT) method as implemented in VASP [1]. The projector-augmented wave method is used with an energy cutoff of 650 eV. The exchange-correlation functional is approximated with the generalized gradient approximation (GGA) and Dudarev's scheme [2] is used to include correlation corrections with an effective correlation strength of *U*eff = 5 eV. K-point meshes of size 8×8×6 and 8×5×6 are used for the room-temperature (P63-*mmc* unit cell) and low-temperature (*Cmcm* unit cell) structures, respectively, both for barlowite and claringbullite. For our calculations with *Pnma* symmetry, we have used the similar k-point mesh as used for *Cmcm*.

[1] Kresse G. and Hafner J., *Ab initio molecular dynamics for liquid metals* Phys. Rev. B **47**, 558 (1993). doi: https://link.aps.org/doi/10.1103/PhysRevB.47.55

[2] Dudarev S. L., Botton G. A., Savrasov S. Y., Humphreys C. J., and Sutton A. P., *Electron-energy-loss spectra and the structural stability of nickel oxide: An LSDA+U study* Phys. Rev. B **57**, 1505 (1998). doi: https://link.aps.org/doi/10.1103/PhysRevB.57.1505

Supplemental Figures

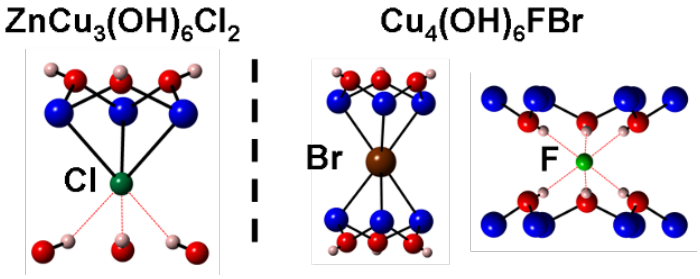

Figure S1. (left) The coordination environment of the interlayer chloride site in herbertsmithite. (right) Two distinct halogen sites in barlowite. Color scheme: Cl = dark green, Cu = blue, O = red, H = salmon, Br = brown, and F = light green.

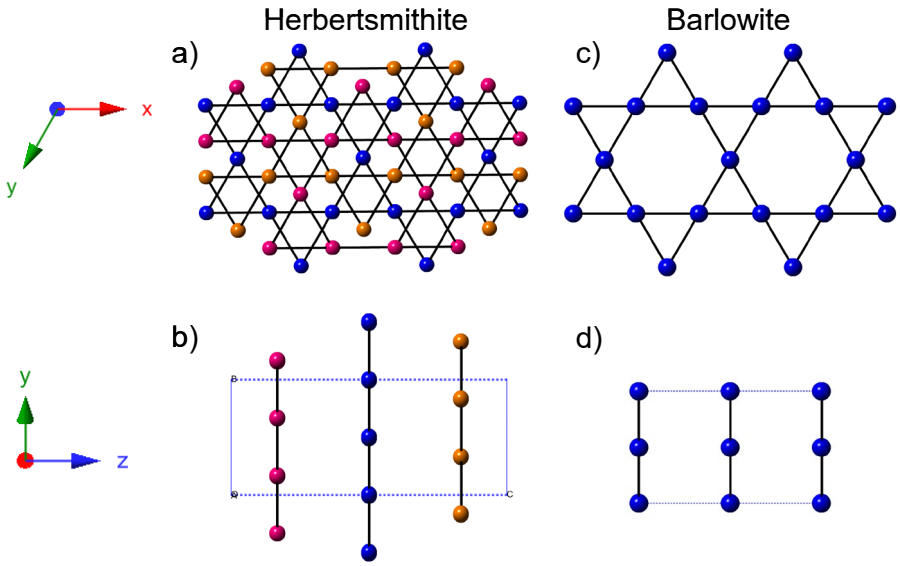

Figure S2. Different stackings of kagome layers. In herbertsmithite (a,b), there are three layers per unit cell along the *c*-axis. For clarity, the copper sites in adjacent layers are illustrated in different colors. In barlowite and claringbullite (c,d), the kagome layers reside directly above each other along the *c*-axis.

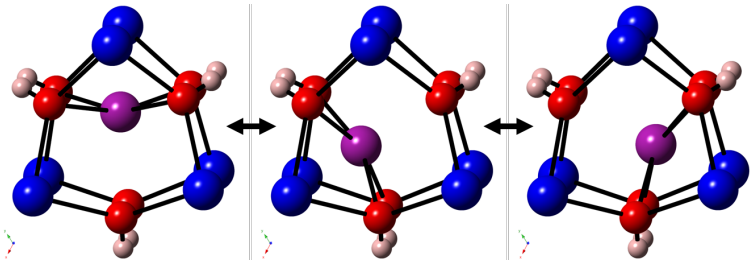

Figure S3. The three possible coordination modes of the interlayer copper site. Above the lock-in temperature, the copper ion fluctuates among these three sites. Purple: copper (interlayer), Blue:

copper (kagome), Red: oxygen, Salmon: hydrogen. Above the lock-in temperature, the copper ion fluctuates among these three sites

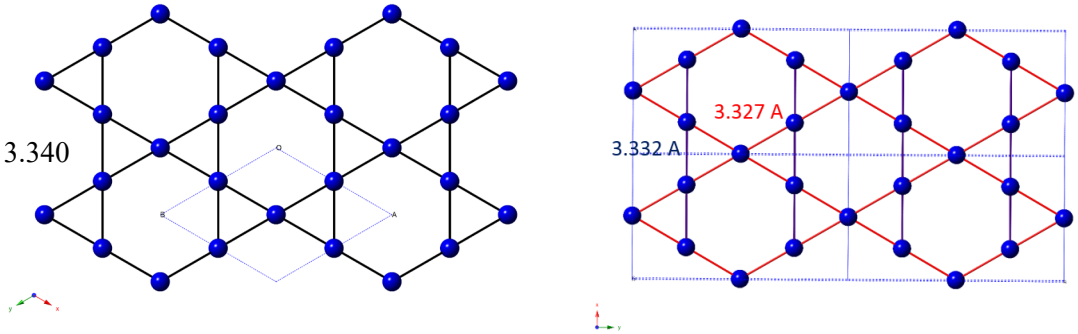

Figure S4. (Left) At room temperature, barlowite crystallizes in the hexagonal *P6₃/mmc* space group and has a prefect kagome lattice. (Right) As the temperature is lowered, a distortion to the orthorhombic *Cmcm* space group is observed, with a corresponding distortion in the kagome layer.

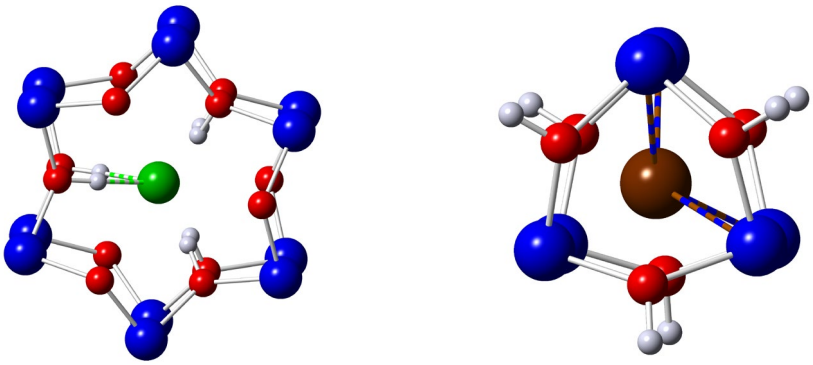

Figure S5. In the low temperature orthorhombic structure, the fluoride ion forms two hydrogen bonds (shown) of 1.737 A. The remaining four H-F interactions expand to 1.829 A. In the orthorhombic structure, the bromide anion also chooses one of three possible coordination environments, with four short (3.007 A) and two long (3.011 A) Cu-Br bonds.

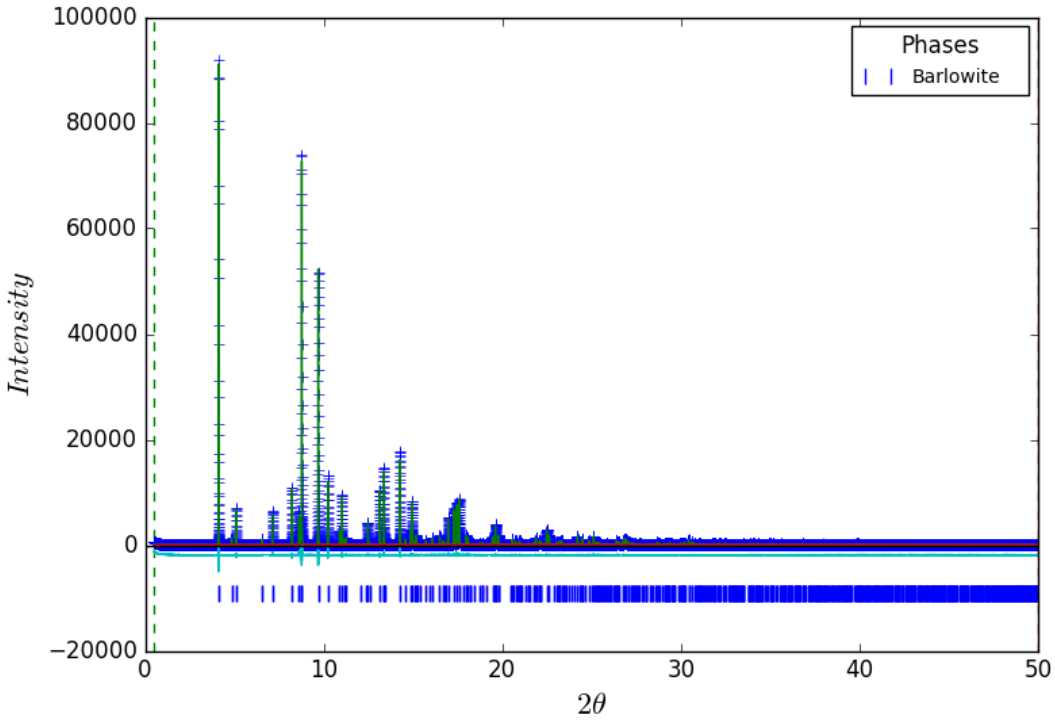

Figure S6. APS X-ray powder diffraction data for barlowite at ambient temperature with GSAS-II refinement.

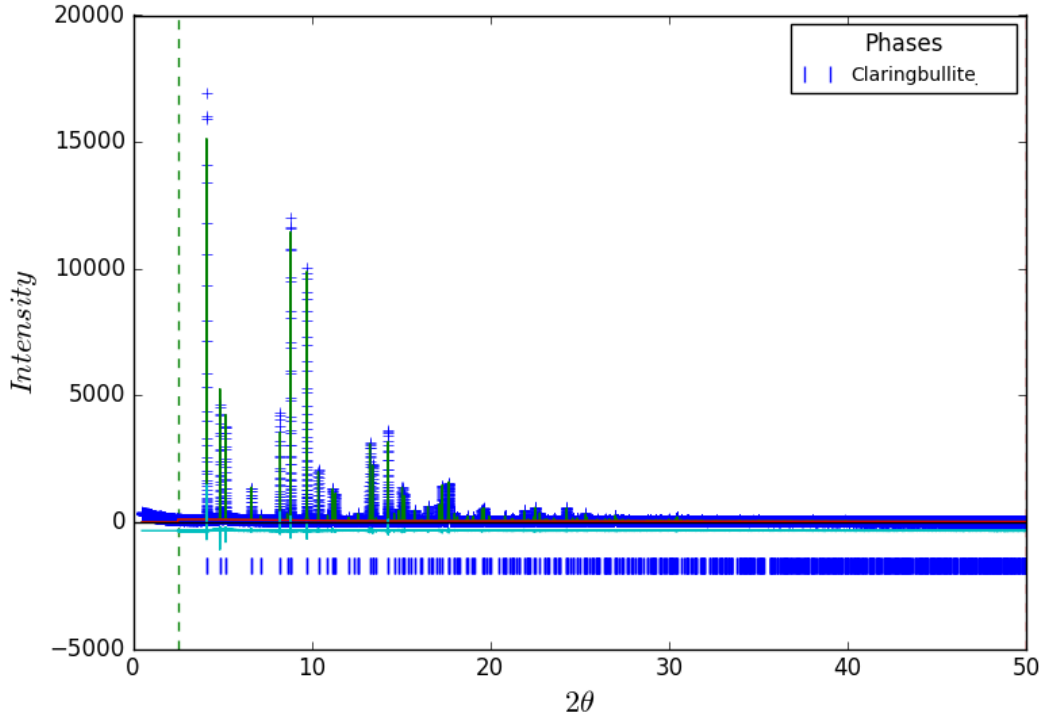

Figure S7. APS X-ray powder diffraction data for claringbullite at ambient temperature with GSAS-II refinement.

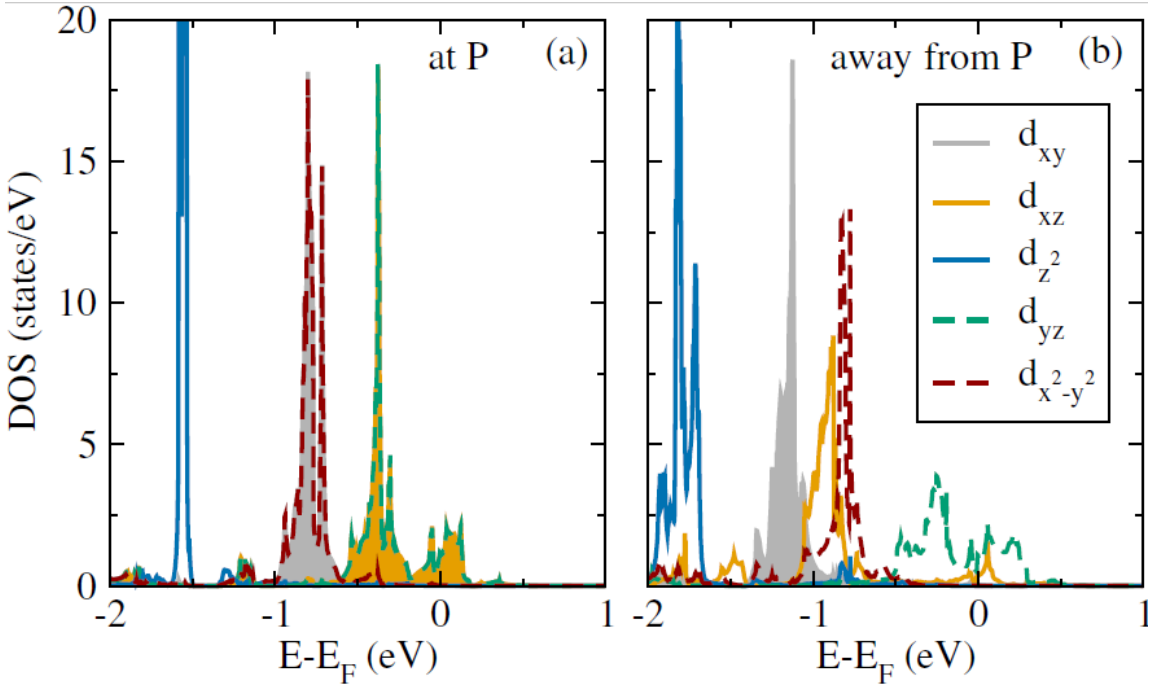

Figure S8. *l*-decomposed partial density of state (DOS) of interlayer Cu^{2+} ion in barlowite (a) at position P and (b) when away from P. The results suggest that these materials undergo a 'Jahn-Teller like distortion' due to the instability caused by the electronic degeneracy between two sets of d-orbitals of the interlayer Cu^{2+} ion at the position P with point group symmetry C_{3v} (Figure S7a). Thus, the system becomes unstable with respect to the nuclear motion away from P in such a way that this degeneracy is lifted; this is evident from Figure S7b.

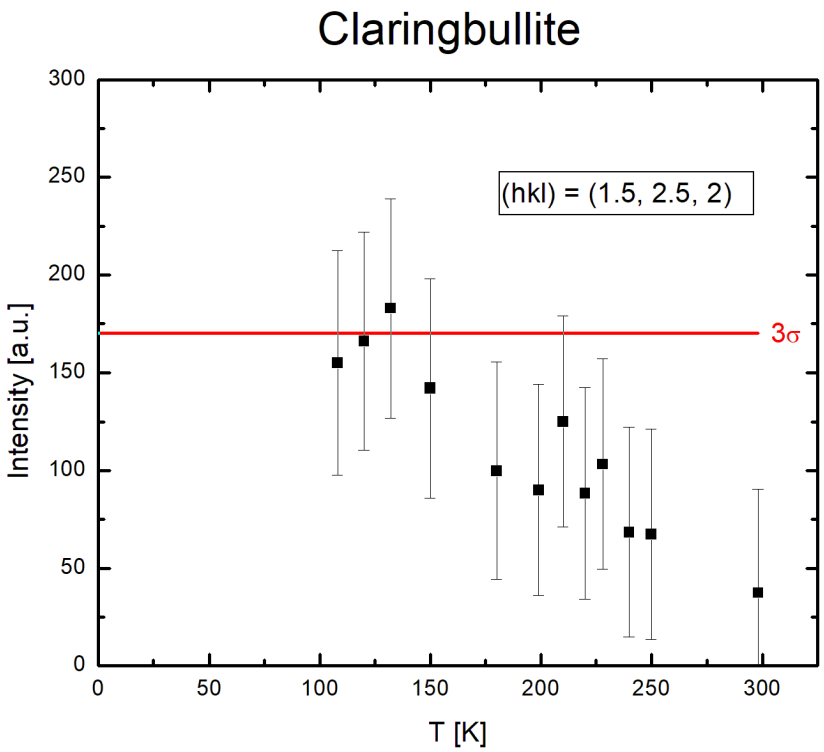

Figure S9: Temperature dependence of the integrated intensity of the superstructure reflection (1.5, 2.5, 2) for a single crystal of claringbullite, obtained from integration of the intensity observed in the CCD frame. The red line indicates the 3σ of the observed integrated background intensity, demonstrating that the observed superstructure intensity is weak, of the order of the background signal.

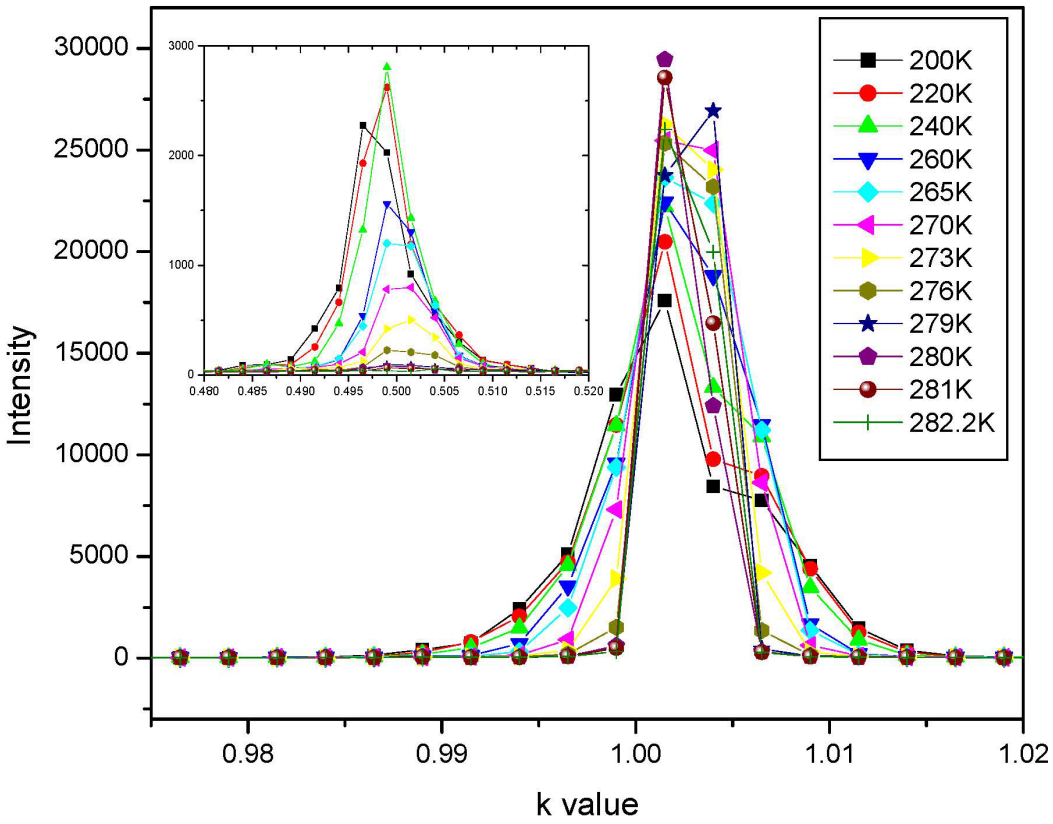

Figure S10. k and T dependence of the intensity of the substructure reflection (-2, 1, 0) and superstructure reflection (-2, 0.5, 0) (inset) for a single crystal of barlowite. The peak broadening of the substructure reflection can be seen.

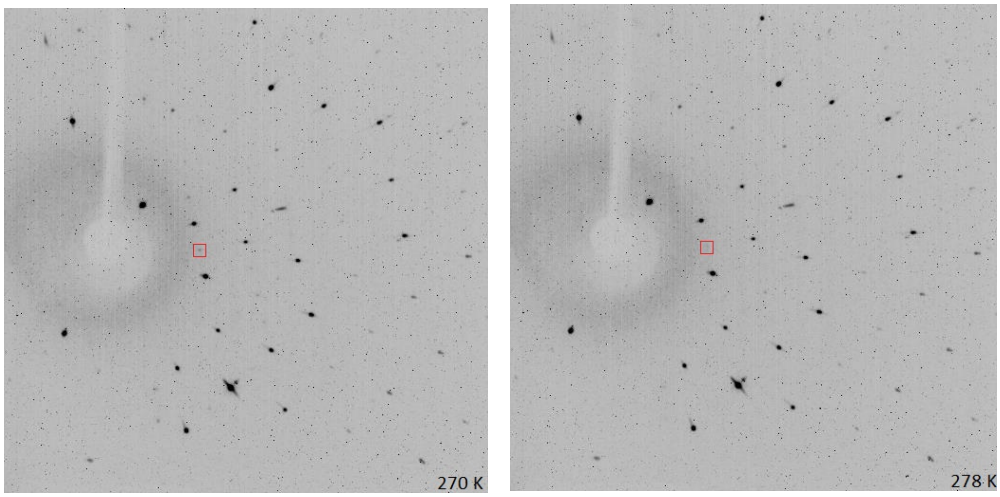

Figure S11. The superstructure peak highlighted in the box is visible at 270 K, but vanishes at 278 K for barlowite. This is consistent with our findings of a "soft" onset of the Cu atom ordering at 276 K.